# Model of a Drive System for Low-Floor Trams with a Four-Linkage Coupling

Henryk SANECKI[1] , Tomasz CZAUDERNA[2]

**Summary**

The article describes the structure and principles of operation of a drive system used in some low-floor trams. The system consists of electric motors, gear transmissions as well as hollow shafts and four-linkage couplings causing the wheels to move. During the study, a dynamic model was built and the parameters needed to carry out a simulation were determined. NGT6 low-floor tram wagons operated by MPK S.A. Cracow were used as examples of existing vehicles. Due to the lack of available data, part of the work was devoted to determining mass moments of inertia of drive system components using an experimental method of torsional vibrations of a string. In subsequent chapters, a mathematical model was developed and a tram start-up simulation was performed based on specific parameters of the individual system components. Some of the results were presented in the form of graphs.

**Keywords:** tram riding simulation, mathematical model of dynamics, start-up, mass moments of inertia, method of torsional vibration of string

## 1. Introduction

The subject matter of the following article revolves around the presentation of a simulation of the operation of a drive system of a low-floor tram with four-linkage couplings [1, 2]. The drive systems of low-floor trams are among the most complex ones used in contemporary railway vehicles, as they should be characterised by:

- a low floor covering as much of the vehicle underframe as possible,
- a small wheel diameter due to the requirements of the lowest possible floor,
- as low of an impact on the vibration of the environment as possible.

In view of these assumptions, high design requirements are placed on the drive systems of these vehicles. Other criteria, such as durability or efficiency, may be of secondary importance. These requirements necessitate a reduction in the size of the drive systems and complicate the power transmission path. Modern trams use very diverse drive systems. Most of the currently manufactured vehicles are low-floor trams with varying proportions of low-floor space inside the vehicle. The drive systems of fully low-floor trams are the most complex. They are often unconventional, however, they are not the topic of this article.

In the article on trams operated in Cracow (such as Bombardier NGT6, Bombardier NGT8, PESA KRAKOWIAK 2014N, STADLER TANGO KRAKÓW), the low floor constitutes about 63–80% of the vehicle's interior surface, while a medium-height floor (about 550–600 mm), differing from the low floor by one step stair, is used above the motor bogies. This solution enabled the use of a classic motor bogie with smaller diameter wheels and reduced size of basic components such as motor, transmission and couplings. A complete springing of the motor and transmission was also achieved through the use of a hollow shaft and a system of two, serially connected four-linkage couplings [3], Fig. 1. Due to the design of the low floor, the diameters of the shafts and coupling should be as small as possible while retaining the properties of the transmission of the driving moments.

In order to obtain an adequate mathematical description of the system presented in Chapter 2 (Fig. 3), it is necessary to determine the mass moments of

---

[1] Ph.D., D.Sc.Eng.; Cracow University of Technology, Department of Rail Vehicles and Transport; henryk.sanecki@pk.edu.pl.

[2] M.Sc.Eng.; Doctoral School of Cracow University of Technology; tczauder@mpk.krakow.pl.

inertia of the individual components, and not all of them have shapes that are convenient for calculations. The components of the vehicle drive system are usually rotating parts of irregular shape, and are frequently made up of various substances of different densities. Typically, these are metal-rubber joints as used in four-linkage couplings (Fig. 2).
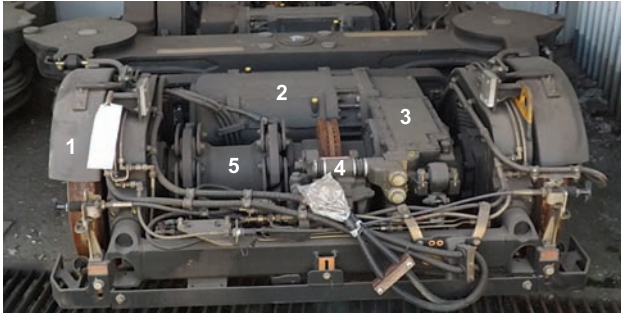


Fig. 1. The drive system of the NGT6 Kr tram car: 1) motor bogie underframe, 2) electric traction motor, 3) transmission, 4) hollow shaft, 5) four-linkage coupling [FLENDER]

Determining mass moments of inertia for complex-shaped components is analytically very difficult, sometimes even impossible, which is why other methods, including experimental ones, are applied. One of these methods is the determination of mass moments of inertia by analysing the torsional vibrations of the string. In such a case, it is important that the string is suspended as an extension of the geometric axis of the tested object in the form of an irregularly shaped rotating solid.

In order to carry out calculations, model dynamic systems are usually modelled using simplifications, which depend on the scope of the system under consideration. In the case of railway vehicles, it is possible to examine the entire body, one of its components, the bogie, the axle with motor and transmission, or to analyse each component in detail.

## 2. A general dynamic model of a drive system

A diagram of a single drive system is shown in Fig. 3a. Their number is $2n_w$, where $n_w$ is the number of motor bogies. The system contains an electric motor with rotor 1.6; 1.1; 1.2 connected to pinion 1.3; 1.4 of a gear transmission via coupling 1.5. The gear transmission consists of gears $z_1$, $z_2$, $z_3$, $z_4$, denoted as 1.4; 2.3; 2.2; 3.2. Then, the driving moment is transmitted to coupling 5 via bush 3, on which elements 3.1-3.6 are located. The bush 3.4 is connected to the middle part of coupling 5 via disc 3.6 and linkages 4 using flexible elements. On the other side of the coupling are linkages 6, flexible elements and disc 7.1, which transmits the driving moment to axle 7.2 and road wheels 7.3 and 7.4.
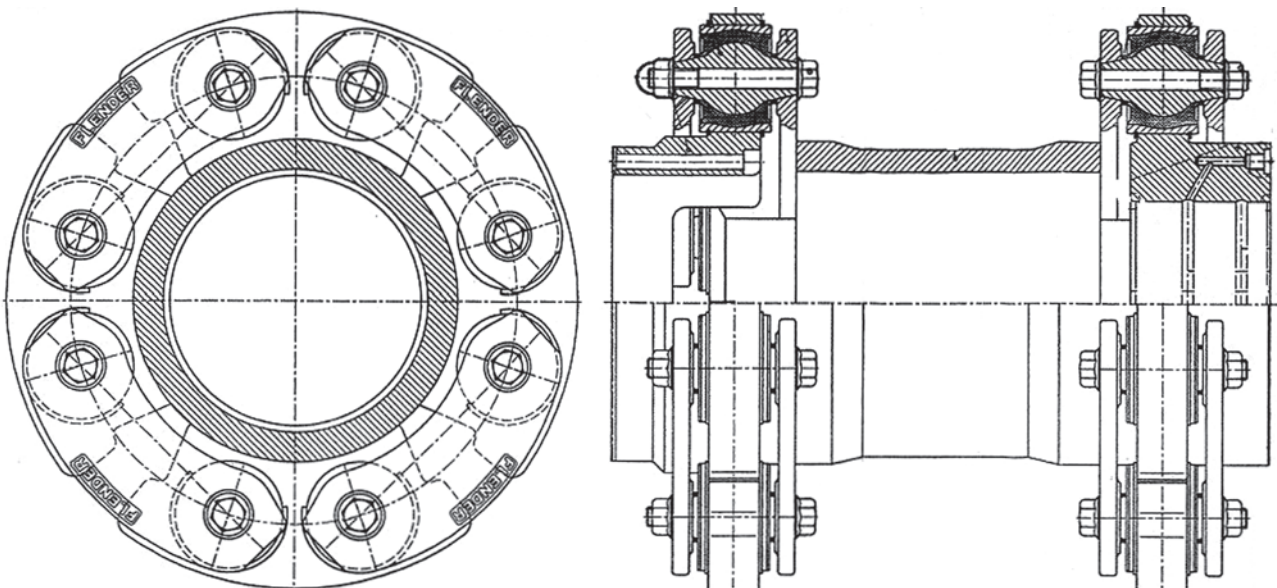


Fig. 2. FLENDER four-linkage coupling used in the drive system of a low-floor tram [1]
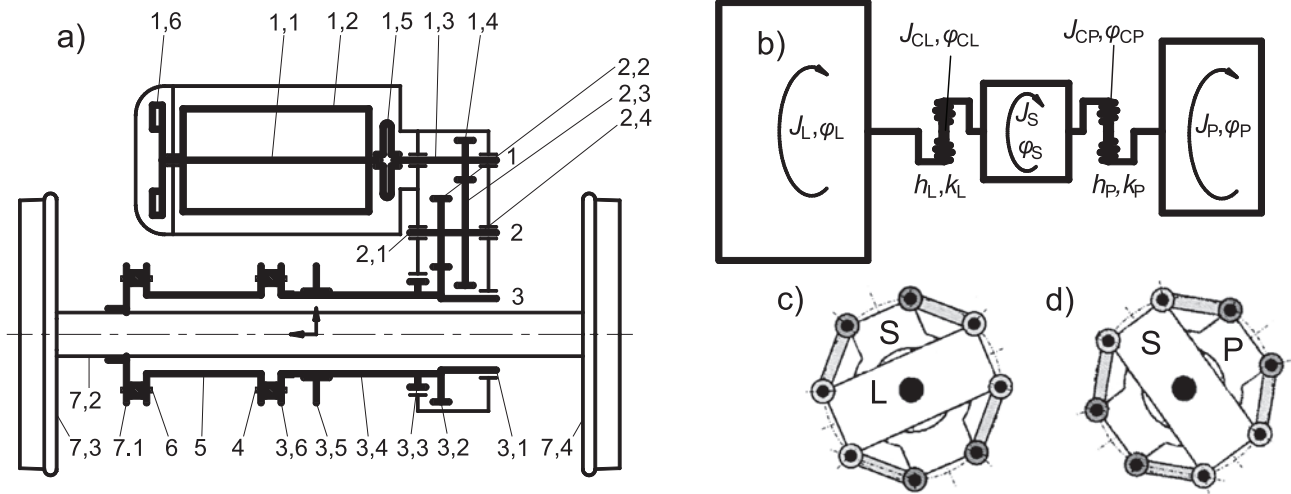
Fig. 3. a) Diagram of a single drive system in the bogie; gears $z_1$, $z_2$, $z_3$, $z_4$ marked as: 1.4; 2.3; 2.2; 3.2; b) substitute model of the tram's drive system; c) connection of the substitute mass L to the coupling centre – layshaft; d) connection of the coupling centre (layshaft) to substitute mass P [own elaboration]

Due to a large number of components in the system under study, the achievement of a viable solution for its dynamics is very difficult. Therefore, the need for some simplifications arises. Figure 3b shows a diagram of a reduced model of a drive system consisting of the following masses: L – left side with respect to the coupling, P – right side with respect to the coupling, S – middle part of the coupling, CL – left-hand linkages of the coupling, CP – right-hand linkages of the coupling. Flexible elements with stiffnesses $k_L$ and $k_P$ and damping coefficients $h_L$ and $h_P$ are on both sides of the coupling.

In the case of the analysed system, the parameters of its real components, as in Fig. 3a, should be replaced by the corresponding parameters of components of the substitute model (Fig. 3b). The reduced moment of inertia $J_P$ can be determined by comparing the kinetic energy of reduced mass P with the total kinetic energy of the components replaced by this mass, i.e.:

$$\frac{1}{2}J_P\dot{\varphi}_P^2 = \frac{1}{2}J_1\eta_1^2\dot{\varphi}_1^2 + \frac{1}{2}J_2\eta_1\dot{\varphi}_2^2 + \frac{1}{2}J_3\dot{\varphi}_P^2, \qquad (1)$$

where: indices 1, 2 and 3 are the shaft numbers (Fig. 3a), and $\eta_1$ is the efficiency of one pair of gears. After transformations, the formula was:

$$J_P = J_1\eta_1^2\left(z_2/z_1\right)^2\left(z_4/z_3\right)^2 + J_2\eta_1\left(z_4/z_3\right)^2 + J_3. \quad (2)$$

An analogous procedure applies to the moment of inertia ($J_L$). The kinetic energy of the reduced mass must correspond to the kinetic energy of the components replaced by this mass, that is:

$$\frac{1}{2}J_L\dot{\varphi}_L^2 \cdot n_{nap} = \frac{1}{2}J_7\dot{\varphi}_L^2 \cdot 2n_w + \frac{1}{2}m_{tram}v^2, \qquad (3)$$

where:

$m_{tram} = m_1 + n_{wn}m_{2n} + n_{wt}m_{2t} + m_3$ – total mass of the tram,

$m_1$ – kerb mass of tram without bogies,

$m_{2n}$ – mass of 1 motor bogie,

$m_{2t}$ – mass of 1 trailer bogie,

$n_w = n_{wn} + n_{wt}$ – number of bogies in the tram,

$n_{wn}$ – number of motor bogies,

$n_{wt}$ – number of trailer bogies,

$n_{nap}$ – number of drive systems (in the analysed tram, it is $2n_{wn}$),

$m_3$ – passengers' mass,

$D$ – wheel diameter,

$v$ – tram speed,

$$v = \dot{\varphi}_L D/2. \qquad (4)$$

After substituting formula (4) into (3) and after transformations, the formula for reduced moment of inertia $J_L$ is as follows:

$$J_L = \left[J_7 \cdot 2n_w + m_{tram}\left(D/2\right)^2\right]\frac{1}{n_{nap}}. \qquad (5)$$

The remaining mass moments of inertia of the substitute model can be defined as:

$$J_{CP} = J_4, J_S = J_5, J_{CL} = J_6. \qquad (6)$$

## 3. Analytical determination of mass moments of inertia

Certain components of the drive system under study (shafts, wheels, discs) have simple shapes that can generally be reduced to a truncated cone with a conical hole (Fig. 4). This structure can be described by the following volume formula:

$$V = \frac{\pi l}{12}\left( \frac{D_b^3 - D_a^3}{D_b - D_a} - \frac{d_b^3 - d_a^3}{d_b - d_a} \right), \qquad (7)$$

or

$$V = \frac{\pi l}{12}\left( 4D_{sr}^2 - D_a D_b - 4d_{sr}^2 + d_a d_b \right). \qquad (8)$$
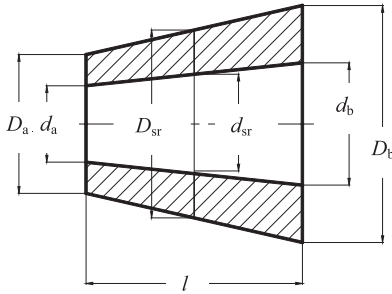
Fig. 4. Dimensions of a truncated cone with a hole
[own elaboration]

The formula for the mass moment of inertia takes the following form:

$$J = \frac{\pi \rho l}{160} \cdot \left( \frac{D_b^5 - D_a^5}{D_b - D_a} - \frac{d_b^5 - d_a^5}{d_b - d_a} \right), \qquad (9)$$

where, to enable calculations for $D_b = D_a$ and/or $d_b = d_a$, it is possible to use the formulae below:

$$\frac{D_b^5 - D_a^5}{D_b - D_a} = \left( D_b - D_a \right)^4 + 5D_b D_a \left( D_b^2 - D_b D_a + D_a^2 \right)$$

$$\frac{d_b^5 - d_a^5}{d_b - d_a} = \left( d_b - d_a \right)^4 + 5d_b d_a \left( d_b^2 - d_b d_a + d_a^2 \right). \qquad (10)$$

## 4. Experimental determination of mass moments of inertia

The mass moment of inertia can be determined using the single-string suspension method. The measuring device consists of a support 1, a string 2, a holder 3 and a tested element 4 (Fig. 5a). The tested specimen is fixed in the holder so that its main axis coincides with the axis of the string. The element suspended from the string is an oscillating system performing torsional vibrations.
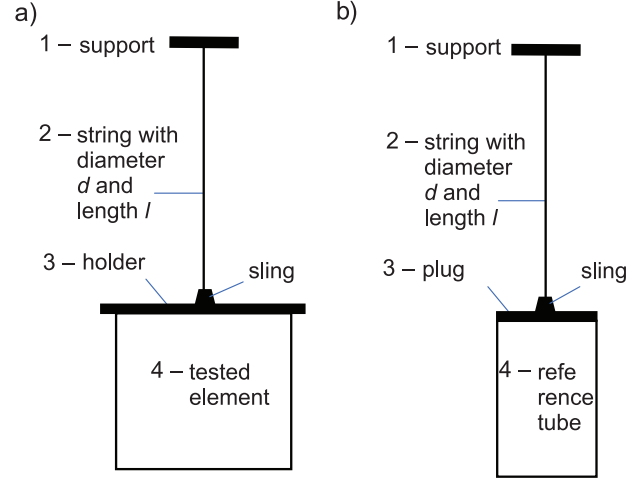
Fig. 5. Diagram of string test site (a), pre-test site (b)
[own elaboration]

### 4.1. Selection of string dimensions

The experiment should be performed using a steel wire, for example, from a music plucked instrument (e.g. an electric guitar). A string of diameter $d$ is loaded with weight $Q$ of the tested element together with a holder, which causes tensile stresses $\sigma = \dfrac{Q}{A}$ and torsional moment $M$, which leads to torsional stresses $\tau = \dfrac{M}{W_o}$. The following strength condition must be met:

$$\sqrt{\sigma^2 + 3\tau^2} = \sqrt{\left(\frac{Q}{A}\right)^2 + 3\left(\frac{M}{W_o}\right)^2} \leq \frac{R_m}{S}, \qquad (11)$$

where:

$A = \dfrac{\pi d^2}{4}$, $W_o = \dfrac{2J_o}{d} = \dfrac{\pi d^3}{16}$,

$R_m$ – tensile strength of the string material,
$S$ – safety factor.

For a given (maximum) angle φ, the torsional moment of the string is:

$$M = \frac{\varphi G J_o}{l} = \frac{\varphi G W_o d}{2l}, \qquad (12)$$

where:

$l$ – distance between the string fixing points,
$G$ – Kirchhoff's modulus; modulus of form elasticity.

Now the strength condition takes the following form:

$$\sqrt{\left(\frac{4Q}{\pi d^2}\right)^2 + 3\left(\frac{\varphi G W_o d}{W_o 2l}\right)^2} = \sqrt{\left(\frac{4Q}{\pi d^2}\right)^2 + 3\left(\frac{\varphi G d}{2l}\right)^2} \le \frac{R_m}{S},$$

(13)

or

$$3\left(\frac{\varphi G}{2l}\right)^2 d^6 - \left(\frac{R_m}{S}\right)^2 d^4 + \left(\frac{4Q}{\pi}\right)^2 \le 0.$$

(14)

By assuming:

$$x = d^2 \ \text{oraz} \ \alpha = 3\left(\frac{\varphi G}{2l}\right)^2, \ \beta = -\left(\frac{R_m}{S}\right)^2, \ \delta = \left(\frac{4Q}{\pi}\right)^2,$$

(15)

an algebraic equation of the third degree is obtained and takes the form:

$$\alpha x^3 + \beta x^2 + \delta = 0.$$

(16)

Equation (16) for $x$ and $d$ can be solved numerically. The required diameter $d = 0{,}85$ mm (assumed to be 1.2 mm) was obtained after calculations for the data:
$E = 210$ GPa, $\nu = 0{,}3$, $G = \dfrac{E}{2(1+\nu)}$, $R_m = 1600$ MPa
and for $Q = 304$ N, $l = 750$ mm, $\varphi = 5°$ and for safety factor $S = 3$.

## 4.2. Theoretical basis of research

Before the actual research is carried out, it is necessary to perform a number of preliminary activities. A string of diameter $d$ should be fixed relative to the suspension point so that its upper end is not rotated or otherwise displaced (this point should be firmly attached). A trial test should be subsequently carried out on an object in the form of a plugged pipe of mass $m_r$, diameter $D_r$ and wall thickness $s_r$ together with a sling, rotating the pipe by an angle $\varphi = 5°$ and measuring the initial vibration period $T_w$ (Fig. 5b). This allows the calculation of moment of inertia $J_w$:

$$J_w = \frac{G T_w^2 J_o}{4\pi^2 l},$$

(17)

where: $J_o = \dfrac{\pi d^4}{32}$.

On the other hand, the moment of inertia for the trial test can be determined theoretically. Taking into account a circular disc (plugging the pipe) of mass $m_T$, diameter $D_T$ and a sling ($J_z$), moment $J_{wt}$ is described by the formula:

$$J_{wt} = \frac{1}{8} m_r \left[ D_r^2 + (D_r - 2s_r)^2 \right] + \frac{1}{8} m_T D_T^2 + J_z,$$

(18)

which allows calculating period $T_{wt}$ and assessing the error $\dfrac{T_w - T_{wt}}{T_w}$:

$$T_{wt} = 2\pi \sqrt{\frac{l J_{wt}}{G J_o}}$$

(19)

It was found that $T_w = 3{,}2$ s with an error of 7,6% and moment of inertia $J_w = 5687$ kg·mm².

In order to carry out the actual tests, a disc (holder 3 with a sling) used for fixing the tested elements should be suspended from the lower end of the string (Fig. 5a). The end of the string must be located at the centre of gravity of the disc so that it occupies a horizontal position. It is necessary to attach successive test objects to the disc and determine the corresponding torsional fluctuation periods $T_i$. On this basis, the mass moments of inertia of the $i$ elements under study can be determined according to the formula:

$$J_i = \frac{T_i^2 G J_o}{4\pi^2 l} - J_u,$$

(20)

where: $J_u$ is the mass moment of inertia of the holder (disc), which can be calculated based on formula (21):

$$J_u = \frac{1}{12} m_u \left[ A_u^2 + B_u^2 \right],$$

(21)

where:
$m_u$ – handle mass,
$A_u, B_u$ – dimensions of the rectangular disc (holder).

## 4.3. Test course

The practical determination of mass moments of inertia was not easy. Initially, the availability of drive system components posed a problem. For this purpose, it is possible to use either brand-new components or components dismantled during periodic repairs. In this case, a brand-new layshaft and centre disc were used, the latter of which is pressed onto the axle shaft under operating conditions. In addition, a test was also carried out on the centre disc from the element unscrewed from shaft one, that is the output shaft on the transmission side. All items were weighed on an electronic scale.

The next step was to select an appropriate string and find a location for the test site. For this purpose,

a gridded staircase was chosen for the platform used to repair components on the roof of railway vehicles. In order to suspend the string, a steel plate with five holes drilled in it was prepared: four for screws passing through the existing holes in the metal-rubber bushes of the tested coupling and one in the centre for screwing in a screw with the test string soldered in. The screw was drilled along the geometric axis and the string was inserted in this place using a hard-soldered joint.

In order to determine the mass moment of the layshaft, i.e. the output shaft on the transmission side, it proved necessary to run three tests (for organisational reasons, at considerable intervals) to achieve results suitable for analysis.

The thickest copper-braided guitar string available was originally chosen. The copper braid caused the layshaft rotation to be significantly greater than 90 degrees each way and not be dampened. It is likely that the elastic potential energy of the braid was revealed.

The second trial involved the thickest thin piano string wire available, with a diameter of 0.56 mm. In general, tests on the reference pipe went correctly except for the undesirable effects of the pendulum, while the shaft testing experienced wire breakage after the first full rotation.

The third attempt yielded the expected results (Fig. 6) apart from the fact that it was not possible to completely eliminate pendulum oscillation, particularly in the case of the test pipe. In the third set of tests, steel (piano) wire with a diameter of 1,2 mm was applied, which allowed testing of all three coupling components correctly. The observed vibration periods increased in proportion to the square of the wire diameter.

The primary accuracy limitations stem from the visual assessment with a measurement accuracy on a film of up to 1 s. An increase in the accuracy of the time scale was not justified, as it was difficult to visually pinpoint the precise moment of turn of the rotational movement of the tested object. The oscillation period was designated as an average from a longer observation interval after eliminating the first less precise movement. For organisational reasons, the measurement was shortened to about three minutes, which translates to a dozen rotations. Other disturbances included vibrations caused by other machines operating inside the hall and vibrations resulting from the mere act of suspending an object or setting it in motion. The mere suspension of an object is an indefinite movement and so is putting it into rotation, which is why the first two or three rotations were excluded from the calculation.

A visual assessment of the recorded digital footage was carried out, with the accuracy of the time measurement being 1 s. In the case of the test pipe, 15 torsional vibrations lasting 48 s were observed, which gives an average of 3,2 s. In the case of the largest component tested, it was five cycles for 142 s, an average of 28,4 s. In two other cases, eight cycles were observed for 204 s, averaging 20,5 s, and five cycles for 114 s, or 19,8 s.
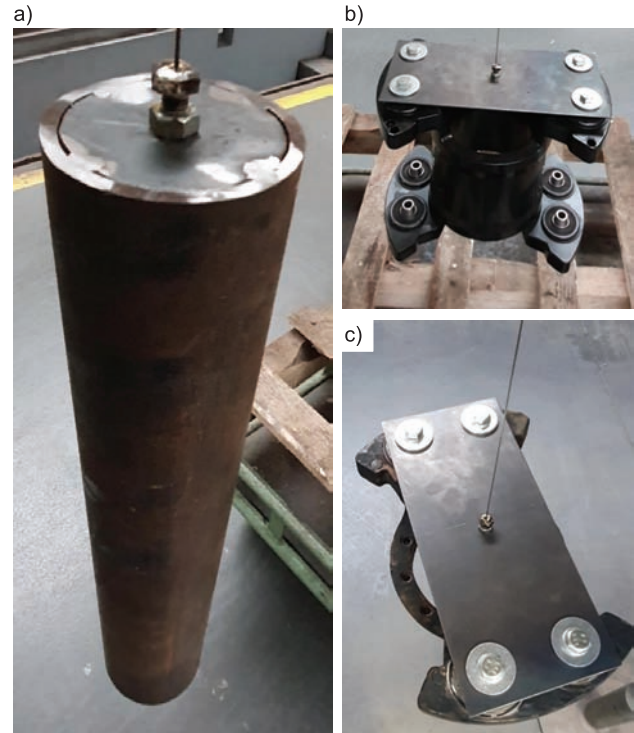


Fig. 6. Experimental determination of the mass moment of inertia: a) of the test tube, b) of the centre section of the coupling, c) of the coupling centre disc on the drive shaft side coming out of the transmission [photo by T. Czauderna]

An additional indication of test accuracy is a comparison of the mass moment of inertia determined analytically and experimentally for the reference pipe under examination.

## 5. Dynamic model

Solutions for various drive systems can be found in many publications, e.g. [4, 5, 6]. The operation of the drive system shown in Fig. 3b is described by the following differential equations:

$$J_L\ddot{\varphi}_L = h_L\left(\dot{\varphi}_{CL} - \dot{\varphi}_L\right) + k_L\left(\varphi_{CL} - \varphi_L\right) - M_L\left(\dot{\varphi}_L\right), \quad (22)$$

$$J_{CL}\ddot{\varphi}_{CL} = -h_L\left(\dot{\varphi}_{CL} - \dot{\varphi}_L\right) - k_L\left(\varphi_{CL} - \varphi_L\right) - \\ + h_L\left(\dot{\varphi}_{CL} - \dot{\varphi}_S\right) - k_L\left(\varphi_{CL} - \varphi_S\right), \quad (23)$$

$$J_S\ddot{\varphi}_S = h_L\left(\dot{\varphi}_{CL} - \dot{\varphi}_S\right) + k_L\left(\varphi_{CL} - \varphi_S\right) + \\ + h_P\left(\dot{\varphi}_{CP} - \dot{\varphi}_S\right) + k_P\left(\varphi_{CP} - \varphi_S\right), \quad (24)$$

$$J_{CP}\ddot{\varphi}_{CP} = -h_P\left(\dot{\varphi}_{CP} - \dot{\varphi}_P\right) - k_P\left(\varphi_{CP} - \varphi_P\right) - \\ + h_P\left(\dot{\varphi}_{CP} - \dot{\varphi}_S\right) - k_P\left(\varphi_{CP} - \varphi_S\right), \quad (25)$$

$$J_P\ddot{\varphi}_P = h_P\left(\dot{\varphi}_{CP} - \dot{\varphi}_P\right) + k_P\left(\ddot{o}_{CP} - \ddot{o}_P\right) + M_P\left(\dot{\varphi}_P\right), \quad (26)$$

where:
- $M_L\left(\dot{\varphi}_L\right)$ denotes a reduced moment caused by the tram's drag forces,
- $M_P\left(\dot{\varphi}_P\right)$ indicates the reduced drive moment from the electric motor.

The anti-torque is described by the following equation (27):

$$M_L\left(\dot{\varphi}_L\right) = F_{op}\left(v\right)\frac{D}{2} = F_{op}\left(\frac{D}{2}\dot{\varphi}_L\right)\frac{D}{2}, \quad (27)$$

where:
- $v$ – tram speed in km/h (maximum 80 km/h), formula (4),
- $F_{op}\left(v\right)$ – the drag force of the tram, which is measured in various ways, is described, for example, in [6]. Fig. 7 shows example diagrams of this function according to various authors.

Further analyses were carried out based on the Davis equation in the form:

$$F_{op}\left(v\right) = a + bv^2 \quad [\text{kN}], \quad (28)$$

where:

$$a = \left(3{,}58 + \frac{14{,}2}{m_{osi}}\right)\cdot\frac{g\cdot m_{tram}}{1000},$$

$$b = 0{,}045\cdot 0{,}151\cdot\frac{S_{czoł}}{m_{osi}n_{wag}}\cdot\frac{g\cdot m_{tram}}{1000}, \quad (29)$$

$v$ – In km/h, $n_{wag} = 3$ – number of elements (carriages) of the tram,
$S_{czoł} = 5{,}52 \text{ m}^2$ – tram front area,
$g\cdot m_{tram} = 457{,}6 \text{ kN}$ – tram weight,

$$m_{osi} = \frac{m_{tram}}{2n_w} = 7780 \text{ kg} \text{ – tram mass per axle,}$$

$n_w = 3$ – number of bogies ($n_w = n_{wn} + n_{wt} = 2+1$).

Knowing the characteristics of the motor $M_s\left(\omega_s\right)$, where $\omega_s = \dot{\varphi}_P u$, it is possible to determine the reduced driving moment according to the formula:

$$M_P\left(\dot{\varphi}_P\right) = M_s\left(\dot{\varphi}_P u\right)\eta_1^2 u, \quad (30)$$

where:
- $u = (z_2/z_1)\cdot(z_4/z_3) = 5{,}0556$, $\eta_1 = 0{,}99$,
- $M_s\left(\dot{\varphi}_P u\right)$ – motor driving moment as a function of the angular velocity of the motor shaft $\omega_s = \dot{\varphi}_P u$.

The following data can be used to characterise $M_s(n)$ of the asynchronous motor used, in line with [1]:
$N_n = 125 \text{ kW}$ (nominal motor power; $N_n = M_n\pi n_n/30$),
$M_n = 675 \text{ Nm}$ (nominal motor torque),
$n_n = 1770 \text{ 1/min}$ (rotational velocity corresponding to the nominal motor torque),
$M_k = 880 \text{ Nm}$ (critical motor torque),
$n_o = 4250 \text{ 1/min}$ (maximum motor speed).

The characteristics $M_s(n)$ may be determined after applying the Kloss equation:

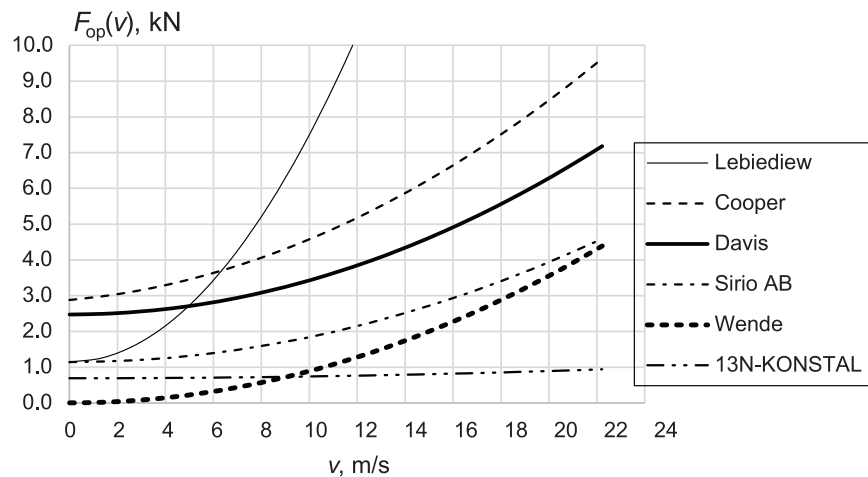$$M_s\left(n\right) = \frac{2ss_k kM_n}{s^2 + s_k^2}, \quad (31)$$



Fig. 7. Diagrams of the $F_{op}(v)$ function for trams according to various authors [6, 7]

where:

$$k = \frac{M_k}{M_n}, \tag{32}$$

$s$, $s_k$ – slippage and critical slippage defined as:

$$s = 1 - \frac{n}{n_o} \ , \ s_k = 1 - \frac{n_k}{n_o}. \tag{33}$$

By using in equation (29) $M_s(n_n) = M_n$ and $s = s_n = 1 - \dfrac{n_n}{n_o}$, the following formula for critical slippage is obtained:

$$s_k = s_n \left( k \pm \sqrt{k^2 - 1} \right). \tag{34}$$

Fig. 8 shows a diagram of function $M_s(n)$ with characteristic quantities, such as $M_r$ – starting torque, $M_n$, $n_n$, $M_k$, $n_k$ and $n_o$, marked.

The Runge-Kutty method can be used to solve the system of equations (22)–(26), which requires new variables:

$$y_0 = \varphi_P, \ y_1 = \dot{y}_0; \ y_2 = \varphi_{CP}, \ y_3 = \dot{y}_2;$$

$$y_4 = \varphi_S, \ y_5 = \dot{y}_4; \ y_6 = \varphi_{CL}, \ y_7 = \dot{y}_6;$$

$$y_8 = \varphi_L, \ y_9 = \dot{y}_8. \tag{35}$$

In addition to the data provided in the previous chapters, the analyses are based on the following quantities:

$m_1 = 20100$ kg – kerb mass of tram without bogies,
$m_{2n} = 4125$ kg – mass of 1 motor bogie,
$m_{2t} = 2650$ kg – mass of 1 trailer bogie,
$n_{wn} = 2$ – number of motor bogies,
$n_{wt} = 1$ – number of trailer bogies,
$m_3 = 15650$ kg – passengers' mass,

$m_{tram} = m_1 + n_{wn} m_{2n} + n_{wt} m_{2t} + m_3 = 46650$ kg – maximum mass of the tram,
$n_{nap} = 2 n_{wn} = 4$ – number of drive systems,
$D = 600$ mm – diameter of a new wheel (minimum value = 510 mm),
$v = 80$ km/h – maximum tram speed,
$k_{11} = 1{,}6648$ kN/mm – radial stiffness of one coupling joint according to [3],
$R = 136$ mm – radius of the circle of arrangement of joint axes in the coupling,
$h_{11}$ – coefficient of damping of one joint in the coupling (at approximately 20°C), in accordance with [8]:

$$h_{11} = (18 \div 42) \left[ LB \cdot \frac{sec}{inch} \right] =$$

$$= (18 \div 42) \left[ 4{,}5 \ N \cdot \frac{sec}{25{,}4 \ mm} \right] =$$

$= (3{,}2 \div 7{,}4)$ [Ns/mm],
$J_7 = 19{,}874$ kg·m$^2$ – mass moment of inertia of the axle set,
$J_L$ – reduced mass moment of inertia at the wheel side, according to formula (5):

$$J_L = \left[ J_7 \cdot 2 n_w + m_{tram} \left( D/2 \right)^2 \right] \frac{1}{n_{nap}} =$$

$$= \left[ 18{,}64 \cdot 2 \cdot 3 + 46650 \cdot \left( \frac{0{,}6}{2} \right)^2 \right] \frac{1}{4} =$$

$$= 1079{,}44 \ kg \cdot m^2$$

$J_{CL} = 0{,}195$ kg·m$^2$ – mass moment of inertia of the linkage system on the left side of the coupling,
$J_S = 0{,}285$ kg·m$^2$ – mass moment of inertia of the central part of the coupling,
$J_{CP} = 0{,}195$ kg·m$^2$ – mass moment of inertia of the linkage system on the right side of the coupling,
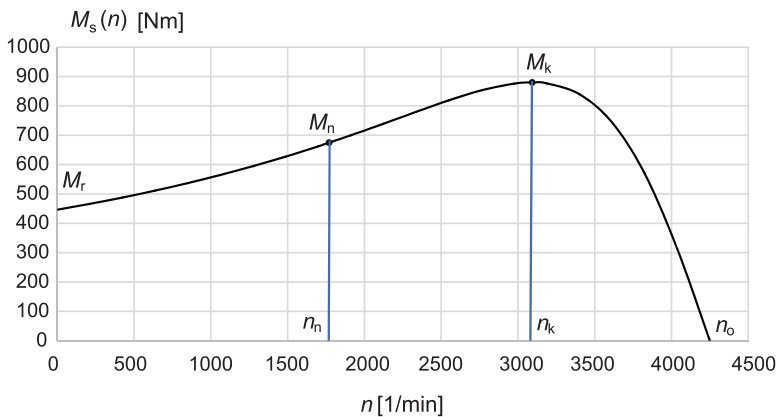$J_P = 24{,}914$ kg·m$^2$ – reduced mass moment of inertia on the motor side,



Fig. 8. Motor characteristics – diagram of function $M_s(n)$ [own elaboration]

$k_{\mathrm{L}} = k_{\mathrm{P}} = 4k_{11}R^2 = 4\cdot1664,8\cdot136^2 = 123,2$ kN·m – rotational stiffness of the linkage system,

$h_{\mathrm{L}} = h_{\mathrm{P}} = 4h_{11}R^2 = 4\cdot(3,2\div7,4)\cdot136^2 = (237\div547)\cdot$kN·s·mm – coefficient of damping of the linkage system.

In order to make the notation dimensionless, it is necessary to use substitution

$$x = t/t_1, \tag{36}$$

where: $t$ – time in s, $t_1$ – auxiliary figure (equal to 1s). This has resulted in the following relationships:

$$\dot{\varphi}_Z = \frac{d\varphi_Z}{dt} = \frac{d\varphi_Z}{dx}\cdot\frac{dx}{dt} = \varphi'_Z\cdot\frac{1}{t_1},$$

$$\ddot{\varphi}_Z = \frac{d^2\varphi_Z}{dt^2} = \frac{d}{dx}\left(\varphi'_Z\cdot\frac{1}{t_1}\right)\cdot\frac{1}{t_1} = \varphi''_Z\cdot\frac{1}{t_1^2}, \tag{37}$$

where: $\varphi_Z$ denotes generally: $\varphi_{\mathrm{P}}$, $\varphi_{\mathrm{CP}}$, $\varphi_{\mathrm{S}}$, $\varphi_{\mathrm{CL}}$, lub $\varphi_{\mathrm{L}}$.

After dividing equations (22)-(26) by $k = k_{\mathrm{L}} = k_{\mathrm{P}}$ on both sides and taking into account the relationship $h = h_{\mathrm{L}} = h_{\mathrm{P}}$, they take the form:

$$\frac{J_{\mathrm{L}}}{kt_1^2}\varphi''_{\mathrm{L}} = \frac{h}{kt_1}\left(\varphi'_{\mathrm{CL}} - \varphi'_{\mathrm{L}}\right) + \left(\varphi_{\mathrm{CL}} - \varphi_{\mathrm{L}}\right) - \frac{M_{\mathrm{L}}\left(\varphi'_{\mathrm{L}}/t_1\right)}{k}, \tag{38}$$

$$\frac{J_{\mathrm{CL}}}{kt_1^2}\varphi''_{\mathrm{CL}} = -\frac{h}{kt_1}\left(2\varphi'_{\mathrm{CL}} - \varphi'_{\mathrm{L}} - \varphi'_{\mathrm{S}}\right) - \left(2\varphi_{\mathrm{CL}} - \varphi_{\mathrm{L}} - \varphi_{\mathrm{S}}\right), \tag{39}$$

$$\frac{J_{\mathrm{S}}}{kt_1^2}\varphi''_{\mathrm{S}} = \frac{h}{kt_1}\left(\varphi'_{\mathrm{CL}} + \varphi'_{\mathrm{CP}} - 2\varphi'_{\mathrm{S}}\right) + \left(\varphi_{\mathrm{CL}} + \varphi_{\mathrm{CP}} - 2\varphi_{\mathrm{S}}\right), \tag{40}$$

$$\frac{J_{\mathrm{CP}}}{kt_1^2}\varphi''_{\mathrm{CP}} = -\frac{h}{kt_1}\left(2\varphi'_{\mathrm{CP}} - \varphi'_{\mathrm{P}} - \varphi'_{\mathrm{S}}\right) - \left(2\varphi_{\mathrm{CP}} - \varphi_{\mathrm{P}} - \varphi_{\mathrm{S}}\right), \tag{41}$$

$$\frac{J_{\mathrm{P}}}{kt_1^2}\varphi''_{\mathrm{P}} = \frac{h}{kt_1}\left(\varphi'_{\mathrm{CP}} - \varphi'_{\mathrm{P}}\right) + \left(\varphi_{\mathrm{CP}} - \varphi_{\mathrm{P}}\right) + \frac{M_{\mathrm{P}}(\varphi'_{\mathrm{P}}/t_1)}{k}. \tag{42}$$

Given the symmetry of the coupling, the following equation applies: $J_{\mathrm{CL}} = J_{\mathrm{CP}}$. By substituting into equations (39) and (41) the so-called small parameter ε, defined as:

$$\varepsilon = \frac{J_{\mathrm{CL}}}{kt_1^2} = \frac{J_{\mathrm{CP}}}{kt_1^2} = \frac{0,195}{123,2\cdot1}\left[\frac{\mathrm{kg}\cdot\mathrm{m}^2}{\mathrm{kN}\cdot\mathrm{m}\cdot\mathrm{s}^2}\right] \simeq 1,583\cdot10^{-6} \ll 1 \tag{43}$$

the equations take the form:

$$\varepsilon\varphi''_{\mathrm{CL}} = -\frac{h}{kt_1}\left(2\varphi'_{\mathrm{CL}} - \varphi'_{\mathrm{L}} - \varphi'_{\mathrm{S}}\right) - \left(2\varphi_{\mathrm{CL}} - \varphi_{\mathrm{L}} - \varphi_{\mathrm{S}}\right), \tag{44}$$

$$\varepsilon\varphi''_{\mathrm{CP}} = -\frac{h}{kt_1}\left(2\varphi'_{\mathrm{CP}} - \varphi'_{\mathrm{P}} - \varphi'_{\mathrm{S}}\right) - \left(2\varphi_{\mathrm{CP}} - \varphi_{\mathrm{P}} - \varphi_{\mathrm{S}}\right). \tag{45}$$

All variable functions generally designated as $\varphi_Z$ are developed into a power series around small parameter ε:

$$\varphi_Z = \sum_{i=0}^{\infty}\varepsilon^i\varphi_{Zi}. \tag{46}$$

When the definition (46) is applied in equation (44), it becomes:

$$\sum_{i=0}^{\infty}\varepsilon^{i+1}\varphi''_{\mathrm{CL}i} = \sum_{i=0}^{\infty}\varepsilon^i\varphi''_{\mathrm{CL}(i-1)} =$$

$$= \sum_{i=0}^{\infty}\varepsilon^i\left[-\beta\left(2\varphi'_{\mathrm{CL}i} - \varphi'_{\mathrm{L}i} - \varphi'_{\mathrm{S}i}\right) - \left(2\varphi_{\mathrm{CL}i} - \varphi_{\mathrm{L}i} - \varphi_{\mathrm{S}i}\right)\right], \tag{47}$$

where the following substitution was made:

$$\beta = \frac{h}{kt_1}. \tag{48}$$

The following iterative relationships were obtained from equation (44):

$$0 = -\beta\left(2\varphi'_{\mathrm{CL}0} - \varphi'_{\mathrm{L}0} - \varphi'_{\mathrm{S}0}\right) - \left(2\varphi_{\mathrm{CL}0} - \varphi_{\mathrm{L}0} - \varphi_{\mathrm{S}0}\right), \tag{49}$$

$$\varphi''_{\mathrm{CL}(i-1)} = -\beta\left(2\varphi'_{\mathrm{CL}i} - \varphi'_{\mathrm{L}i} - \varphi'_{\mathrm{S}i}\right) - \left(2\varphi_{\mathrm{CL}i} - \varphi_{\mathrm{L}i} - \varphi_{\mathrm{S}i}\right)$$
$$\text{for } i = 1, 2, 3, \ldots \tag{50}$$

and, after analogous operations on equation (45), compounds:

$$0 = -\beta\left(2\varphi'_{\mathrm{CP}0} - \varphi'_{\mathrm{P}0} - \varphi'_{\mathrm{S}0}\right) - \left(2\varphi_{\mathrm{CP}0} - \varphi_{\mathrm{P}0} - \varphi_{\mathrm{S}0}\right), \tag{51}$$

$$\varphi''_{\mathrm{CP}(i-1)} = -\beta\left(2\varphi'_{\mathrm{CP}i} - \varphi'_{\mathrm{P}i} - \varphi'_{\mathrm{S}i}\right) - \left(2\varphi_{\mathrm{CP}i} - \varphi_{\mathrm{P}i} - \varphi_{\mathrm{S}i}\right)$$
$$\text{for } i = 1, 2, 3, \tag{52}$$

Given the zero approximations (49) and (51), variables $\varphi_{\mathrm{CL}0}$ and $\varphi_{\mathrm{CP}0}$ can be eliminated, hence equations (42), (40) and (38) take the form:

$$\varepsilon_{\mathrm{P}}\varphi''_{\mathrm{P}0} = \frac{\beta}{2}\left(\varphi'_{\mathrm{S}0} - \varphi'_{\mathrm{P}0}\right) + \frac{1}{2}\left(\varphi_{\mathrm{S}0} - \varphi_{\mathrm{P}0}\right) + \frac{M_{\mathrm{P}}\left(\varphi'_{\mathrm{P}0}/t_1\right)}{k}, \tag{53}$$

$$\varepsilon_{\mathrm{S}}\varphi''_{\mathrm{S}0} = \frac{\beta}{2}\left(\varphi'_{\mathrm{L}0} + \varphi'_{\mathrm{P}0} - 2\varphi'_{\mathrm{S}0}\right) + \frac{1}{2}\left(\varphi_{\mathrm{L}0} + \varphi_{\mathrm{P}0} - 2\varphi_{\mathrm{S}0}\right), \tag{54}$$

$$\varepsilon_{L}\varphi_{L0}'' = \frac{\beta}{2}\left(\varphi_{S0}' - \varphi_{L0}'\right) + \frac{1}{2}\left(\varphi_{S0} - \varphi_{L0}\right) - \frac{M_{L}\left(\varphi_{L0}'/t_{1}\right)}{k},$$
$$(55)$$

where the following substitution was made:

$$\varepsilon_{L} = \frac{J_{L}}{kt_{1}^{2}}, \; \varepsilon_{S} = \frac{J_{S}}{kt_{1}^{2}}, \; \varepsilon_{P} = \frac{J_{P}}{kt_{1}^{2}}. \tag{56}$$

In order to solve the system of equations (53)−(55) using the Runge-Kutty method, the following new variables must be applied (with the $i$ index omitted):

$$y_{0} = \varphi_{P}, \; y_{1} = y', \; y_{2} = \varphi_{S}, \; y_{3} = y_{2}',$$

$$y_{4} = \varphi_{L}, \; y_{5} = y_{4}'. \tag{57}$$

Equations (53), (54) and (55) assume the form:

$$y_{1}' = \frac{\beta}{2\varepsilon_{P}}\left(y_{3} - y_{1}\right) + \frac{1}{2\varepsilon_{P}}\left(y_{2} - y_{0}\right) + \frac{1}{k\varepsilon_{P}}M_{P}\left(y_{1}/t_{1}\right),$$
$$(58)$$

$$y_{3}' = \frac{\beta}{2\varepsilon_{S}}\left(y_{5} + y_{1} - 2y_{3}\right) + \frac{1}{2\varepsilon_{S}}\left(y_{4} + y_{0} - 2y_{2}\right), (59)$$

$$y_{5}' = \frac{\beta}{2\varepsilon_{L}}\left(y_{3} - y_{5}\right) + \frac{1}{2\varepsilon_{L}}\left(y_{2} - y_{4}\right) - \frac{1}{k\varepsilon_{L}}M_{L}\left(y_{5}/t_{1}\right).$$
$$(60)$$

To obtain the next (1st) approximation, it can be seen that equations (49) and (51) can be written as:

$$\left[\ln\left(2\varphi_{CL0} - \varphi_{L0} - \varphi_{S0}\right)\right]' = -\frac{1}{\beta}, \tag{61}$$

$$\left[\ln\left(2\varphi_{CP0} - \varphi_{P0} - \varphi_{S0}\right)\right]' = -\frac{1}{\beta}, \tag{62}$$

or

$$2\varphi_{CL0} - \varphi_{L0} - \varphi_{S0} = C_{1}e^{-\frac{x}{\beta}}, \tag{63}$$

$$2\varphi_{CP0} - \varphi_{P0} - \varphi_{S0} = C_{2}e^{-\frac{x}{\beta}}. \tag{64}$$

Assuming zero initial conditions for the angles: $\varphi_{CL0}$, $\varphi_{L0}$, $\varphi_{CP0}$, $\varphi_{P0}$, $\varphi_{S0}$ (for $x = 0$), it is possible to obtain $C_{1} = C_{2} = 0$ and formulas:

$$\varphi_{CL0}'' = \frac{\varphi_{L0}'' + \varphi_{S0}''}{2}, \tag{65}$$

$$\varphi_{CP0}'' = \frac{\varphi_{P0}'' + \varphi_{S0}''}{2}, \tag{66}$$

which determine the left sides of equations (50) and (52), namely (for $i = 1$):

$$\varphi_{CL0}'' = -\beta\left(2\varphi_{CL1}' - \varphi_{L1}' - \varphi_{S1}'\right) - \left(2\varphi_{CL1} - \varphi_{L1} - \varphi_{S1}\right), (67)$$

$$\varphi_{CP0}'' = -\beta\left(2\varphi_{CP1}' - \varphi_{P1}' - \varphi_{S1}'\right) - \left(2\varphi_{CP1} - \varphi_{P1} - \varphi_{S1}\right). (68)$$

The determination of successive approximations for the solution of the problem under study was further abandoned due to the difficulty of expanding functions $M_{P}\left(\varphi_{P}'/t_{1}\right)$ and $M_{L}\left(\varphi_{L}'/t_{1}\right)$ into a power series with respect to small parameter $\varepsilon$. The complication stems from the fact that the listed functions must take forms similar to the right side of the function (46). At this point, it should be noted that it is possible, although very labour-intensive, to obtain such a result, as it requires the approximation of functions $M_{P}\left(\varphi_{P}'/t_{1}\right)$ and $M_{L}\left(\varphi_{L}'/t_{1}\right)$ by 5th- and 2nd-degree polynomials.

An additional argument for omitting successive iterations is a very small value of parameter $\varepsilon$, which can be seen from equation (43). It allows neglecting successive expressions of the expansions of individual functions.

# 6. Results of the simulation of drive system movement

Chapter 6.1 contains the results of a simulation of tram movement: angles of rotation and speeds for the data provided above (fully loaded tram) and for an example of motor torque $M_{st}(\xi)$.

## 6.1. Motor driving moment control

During movement, the motor is controlled to adapt the driving moment to the resistance of the movement so as to achieve the correct tram speed (Fig. 9).

For the intersection of the $n_{x1}$ characteristics $M_{st1}(n)$ and $M_{st2}(n)$, the following condition must be satisfied:

$$M_{st1}(n_{x1}) = M_{st2}(n_{x2}), \tag{69}$$

i.e. (after applying formula [31]):

$$\frac{s_{1}s_{k1}}{s_{1}^{2} + s_{k1}^{2}} = \frac{s_{2}s_{k2}}{s_{2}^{2} + s_{k2}^{2}}, \tag{70}$$

where:

$$s_{i} = 1 - \frac{n}{n_{oi}}, \; s_{ki} = 1 - \frac{n_{ki}}{n_{oi}}, \; i = 1, 2. \tag{71}$$
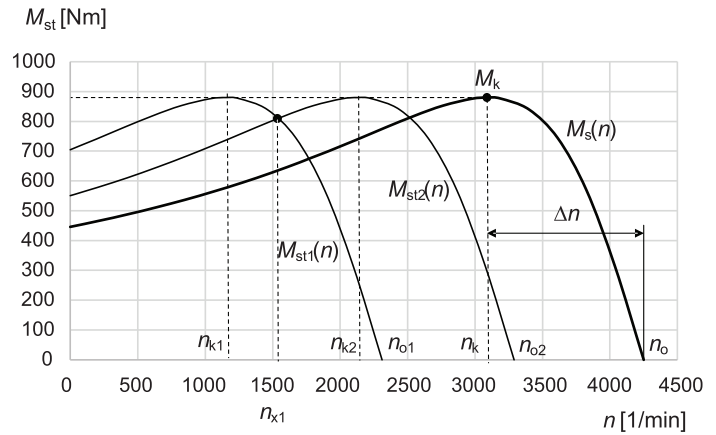
$M_{st}$ [Nm]



Fig. 9. Controlled motor characteristics $M_{st1}(n)$ and $M_{st2}(n)$ intersecting at point $n_{x1}$ and nominal characteristic $M_s(n)$ [own elaboration]

The substitution of formulae (71) into (70) results in the equation:

$$\frac{(n_{o1}-n)\cdot n_{o1}s_{k1}}{(n_{o1}-n)^2 + n_{o1}^2 s_{k1}^2} = \frac{(n_{o2}-n)\cdot n_{o2}s_{k2}}{(n_{o2}-n)^2 + n_{o2}^2 s_{k2}^2}, \quad (72)$$

in which it is necessary to consider relationships:

$$n_{o1}s_{k1} = n_{o2}s_{k2} = n_o s_k = n_o - n_k = \Delta n. \quad (73)$$

Therefore, after appropriate transformations, the following quadratic equation is obtained:

$$(n_{o1}-n)\cdot(n_{o2}-n) - \Delta n^2 = 0, \quad (74)$$

with a root:

$$n_{x1} = \frac{n_{o1}+n_{o2}}{2} \mp \sqrt{\left(\frac{n_{o1}-n_{o2}}{2}\right)^2 + \Delta n^2}. \quad (75)$$

After applying dimensionless variables:

$$\xi = \frac{n}{n_o}, \ \xi_{xi} = \frac{n_{xi}}{n_o}, \ \xi_{oi} = \frac{n_{oi}}{n_o}, \ s_k = \frac{\Delta n}{n_o}, \ i = 1, 2, 3, \quad (76)$$

the solution becomes:

$$\xi_{x1} = \frac{\xi_{o1}+\xi_{o2}}{2} \mp \sqrt{\left(\frac{\xi_{o1}-\xi_{o2}}{2}\right)^2 + s_k^2} \quad (77)$$

or in general:

$$\xi_{xi} = \frac{\xi_{oi}+\xi_{o,i+1}}{2} \mp \sqrt{\left(\frac{\xi_{oi}-\xi_{o,i+1}}{2}\right)^2 + s_k^2}. \quad (78)$$

## 6.2. Tram start-up simulation

The case of motor control using 5 sub-characteristics was analysed. In the case of simulation

calculations, the control moment formula $M_{st}(\xi)$ was used as presented in formula (79). It forms the envelope of partial characteristics $M_{sti}(\xi)$, $i = 1,2,\ldots,5$ shown in Fig. 10 (thick continuous line).

$$M_{st}(\xi) = 2M_k s_k \cdot \left| \begin{array}{l} \dfrac{\xi_{o1}-\xi}{(\xi_{o1}-\xi)^2 + s_k^2} \ \text{if} \ 0 \le \xi \le \xi_{x1} \\[2mm] \dfrac{\xi_{o2}-\xi}{(\xi_{o2}-\xi)^2 + s_k^2} \ \text{if} \ \xi_{x1} \le \xi \le \xi_{x2} \\[2mm] \dfrac{\xi_{o3}-\xi}{(\xi_{o3}-\xi)^2 + s_k^2} \ \text{if} \ \xi_{x2} \le \xi \le \xi_{x3} \\[2mm] \dfrac{\xi_{o4}-\xi}{(\xi_{o4}-\xi)^2 + s_k^2} \ \text{if} \ \xi_{x3} \le \xi \le \xi_{x4} \\[2mm] \dfrac{\xi_{o5}-\xi}{(\xi_{o5}-\xi)^2 + s_k^2} \ \text{if} \ \xi_{x4} \le \xi \le \xi_{x5} \end{array} \right. \quad (79)$$
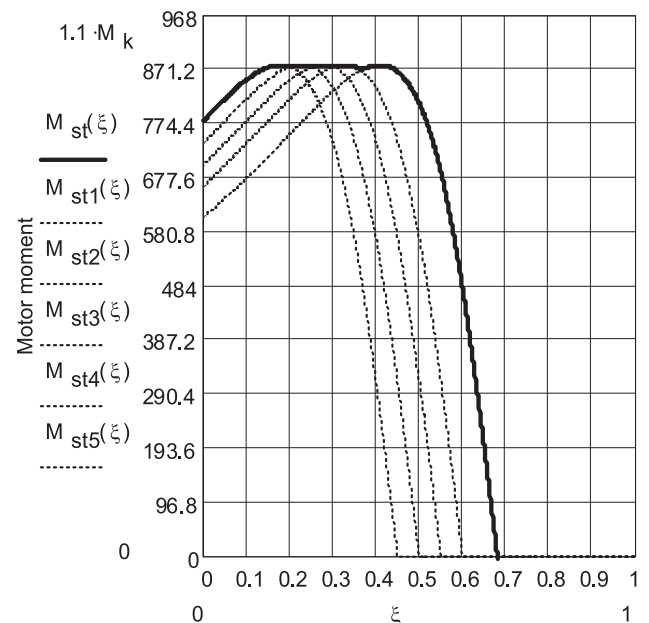


Fig. 10. Cours of motor moment $M_{st}(\xi)$ [own elaboration]
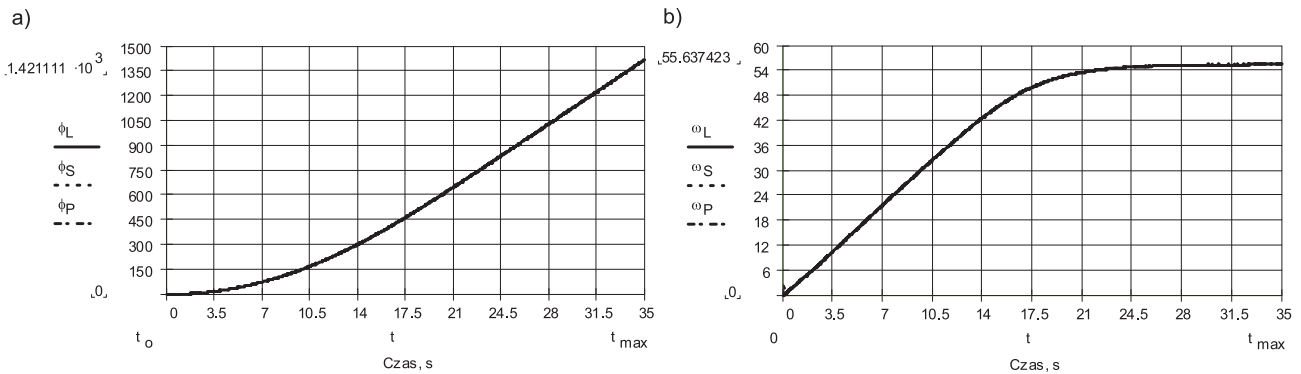
a)

b)

Fig. 11. First seconds (up to 35 s) of the course of change of: a) angles of rotation (in rad): $\varphi_L$, $\varphi_S$, $\varphi_P$; b) angular velocity (in rad/s): $\omega_L = \dot{\varphi}_L$ , $\omega_S = \dot{\varphi}_S$ , $\omega_P = \dot{\varphi}_P$ [own elaboration]
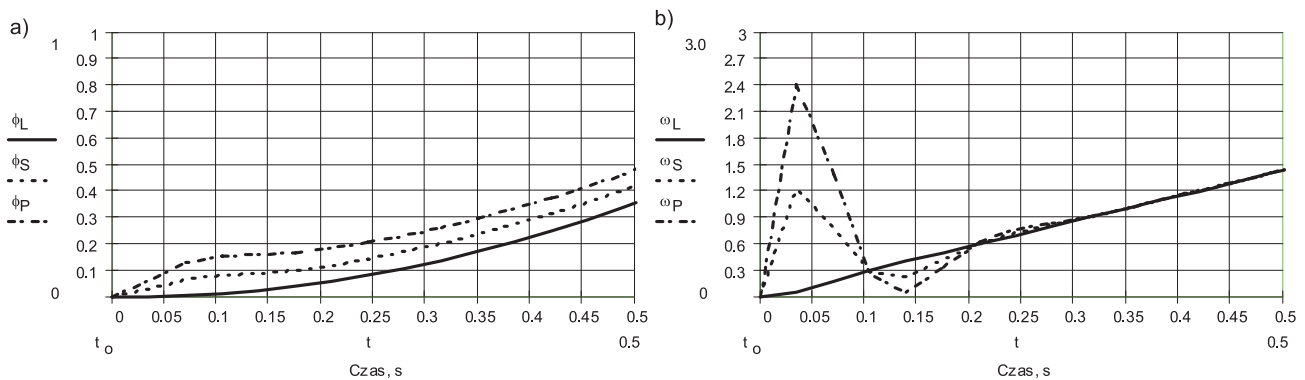
a)

b)

Fig. 12. Initial moments (up to 0,5 s) of the course: a) changes in angles of rotation (in rad): $\varphi_L$, $\varphi_S$, $\varphi_P$; b) angular velocity changes (in rad/s): $\omega_L$, $\omega_S$, $\omega_P$ [own elaboration]

Fig. 11 presents the results of an example simulation of a tram drive system start-up. The graphs show the first 35 seconds of the course of change in angles of rotation (in radians): $\varphi_L$, $\varphi_S$, $\varphi_P$; and angular velocity (in rad/s): $\omega_L = \dot{\varphi}_L$ , $\omega_S = \dot{\varphi}_S$ , $\omega_P = \dot{\varphi}_P$ . The maximum driving speed was 60 km/h and was stabilised for $\xi = n/n_{05} = 0{,}681$. Graphs of similar start-up volumes (up to 0,5 s) are presented in Fig. 12.

## 7. Conclusions

The article describes the construction and principle of operation as well as defines a dynamic model of the drive system, composed of hollow shafts and four-linkage couplings, used in low-floor trams. Due to the lack of available data, an important task was to determine the mass moments of inertia of the drive system components experimentally using a method of torsional vibrations of a string. In the next stage, the start-up of the NGT6 tram was simulated according to specified parameters, followed by the

simulation of torsional vibrations of individual system components.

## References

1. Przekładnia zespołu napędowego. NGT6-1 Obsługa Techniczna OT6, Nr dokumentu: 39_OT6_NGT6-01, Bombardier Transportation.

2. Vossloh Electrical Systems. Kiepe 00 KP 3 DEPI, „Elektryczne wyposażenie niskopodłogowych wagonów tramwajowych NGT6 Miejskiego Przedsiębiorstwa Komunikacyjnego w Krakowie".

3. Czauderna T., Maniowski M.: *Analiza podatności sprzęgła 4-cięgłowego stosowanego w niskopodłogowych tramwajach* [Flexibility analysis of a 4-string coupling used in low-floor trams], Konferencja Naukowo-Techniczna Nowoczesne Technologie w Transporcie Szynowym, Zakopane 2013, 2013.

4. Markusik S., Opasiak T.: *Wpływ błędów montażu sprzęgieł skrętnie podatnych na pracę układu napędowego* [Influence of assembly errors of torsionally sensitive couplings on the operation of the drive

system], Zeszyty Naukowe Politechniki Śląskiej, Seria Transport, tom z. 44, nr 1562, 2002.

5. Krasiński M., Stachoń S.: *Nieustalone drgania w układach napędowych mechanizmu podnoszenia dźwignic w procesie rozruchu przy podnoszeniu ładunku* [Unsteady vibrations in the drive systems of the crane lifting mechanism during the start-up process when lifting the load], Czasopismo Techniczne, Wydawnictwo Politechniki Krakowskiej, Z. 9-M/2008.

6. Biliński J. et. al.: *Opory ruchu tramwajów* [Tram traffic resistance], TTS Technika Transportu Szynowego, Eksploatacja, Tomy 2020, Nr 7−8, s. 64−66.

7. Wende D.: *Fahrdynamik des Schienenverkehrs* [Fahrdynamik des Schienenverkehrs], Vieweg+Teubner Verlag/ Springer Fachmedien Wiesbaden GmbH, 2003.

8. Schaefer R.: *Mechanical properties of rubber*, Chapter 33, [in Harris' Shock and Vibration Handbook], Sixth Edition, 2010, pp. 33.1−33.18.